# A self-adaptive mesh method for the Camassa-Holm equation

Bao-Feng Feng[1], Yasuhiro Ohta[2] and Ken-ichi Maruno[1]

[1] *Department of Mathematics, The University of Texas-Pan American, Edinburg, TX 78539-2999*

[2] *Department of Mathematics, Kobe University, Rokko, Kobe 657-8501, Japan*

**Abstract**

A self-adaptive mesh method is proposed for the numerical simulations of the Camassa-Holm equation based on its integrable semi-discretization. It is an integrable scheme, possessing the $N$-soliton solution (see J. Phys. A, **41** 355205). Moreover, it is called a self-adaptive mesh method, because the non-uniform mesh is driven and adapted automatically by the solution. Once the non-uniform mesh is evolved, the solution is determined by solving a tridiagonal linear system. Due to these two superior features of the method, the numerical results of the propagation and interactions of soliton and cuspons agree with exact ones very well even by a small number of grid points.

June 3, 2009

*Key words:* Camassa-Holm equation, Self-adaptive mesh method, Integrability
*2000 MSC:* 65M06, 35Q58, 37K40

## 1. Introduction

The Camassa-Holm (CH) equation

$$u_T + 2\kappa^2 u_X - u_{TXX} + 3uu_X = 2u_X u_{XX} + uu_{XXX}. \tag{1}$$

has attracted considerable interest since it was derived as a model equation for shallow water waves [1, 2]. When $\kappa = 0$, the CH equation admits peakon solutions which are represented by piecewise functions [3]. When $\kappa \neq 0$, cusped soliton (cuspon) solutions, as well as smooth soliton solutions, were found [4, 5, 6, 7, 8, 9, 10, 11].

Several numerical schemes have been proposed for the CH equation in the literature. These include a pseudospectral method [12], finite difference schemes [13, 14], a finite volume method [15], a finite element method [16, 17], multi-symplectic methods [18], and a particle method based on the formulation in terms of characteristics based on the multi-peakon solution [19, 20, 21, 22, 23]. We comment that the schemes in [13, 14] and in [18] can handle peakon-antipeakon interactions. However, it still remains to be a challenging problem for the numerical integration of the CH equation due to the singularities of cuspon and peakon solutions.

In the present paper, we will study an integrable difference scheme for the CH equation (1) based on an integrable semi-discrete CH equation proposed by the authors [24]. The scheme consists of an algebraic equation between the solution and the non-uniform mesh, and an evolution equation for the mesh. Since the mesh is automatically driven and adapted by the solution, we name it the self-adaptive mesh method hereafter.

As a matter of fact, Harten and Hyman has proposed a self-adjusting grid method for one-dimensional hyperbolic problems [25]. Since then, there has been significant progress in developing adaptive mesh methods for PDEs [26, 27, 28, 29, 30, 31, 32]. These methods have been successfully applied to a variety of physical and engineering problems with singular or nearly singular solutions developed in fairly localized regions, such as shock waves, boundary layers, detonation waves, etc. Recently, an adaptive unwinding method is proposed for the CH equation [15]. The method is high resolution and stable. However, in order to achieve a good accuracy, a large number of grid points ($= 4096$) has to be used. In addition, the designed method is only suitable for the single peakon propagation and peakon-peakon interactions, not for the peakon-antipeakon interaction. As shown subsequently, the self-adaptive mesh method gives a great accuracy by using a small number of grid points ($\approx 100$) for all challenging test problems.

The remainder of this paper is organized as follows. In Section 2, we describe the self-adaptive mesh method and show it converges to the CH equation as the mesh size approaches to zero. Two time advancing methods in implementing the self-adaptive mesh method are presented in Section 3. In Section 4, several numerical experiments, including the propagations of "peakon" and "cuspon" solutions, cuspon-cuspon and soliton-cuspon collisions. The conclusion and remarks are given in Section 5.

## 2. A self-adaptive mesh method for the Camassa-Holm equation

The self-adaptive mesh method we propose for the CH equation (1) is

$$\begin{cases} \Delta^2 w_k = \dfrac{1}{\delta_k} M\left(\delta_k M w_k + \dfrac{1}{c\delta_k}\dfrac{\delta_k^2/c^2 - 4a^2}{1/c^2 - a^2}\right), \\ \partial_t \delta_k = \left(1 - \dfrac{\delta_k^2}{4}\right)\delta_k \Delta w_k \,, \end{cases} \tag{2}$$

where $c = 1/\kappa$. On the grid points $X_k$ with $k = 1, \cdots, N$, the solution $w(X_k, t)$ is approximated by $w_k(t)$. The mesh $\delta_k = X_{k+1} - X_k$ is non-uniform and time-dependent. The parameter $a$ is a small constant which gives the mesh $\delta_k = 2ac$ when the solution $w_k$ remains unchanged. It was shown in [24] that the relation between $a$ and $\delta_k$ implies a discrete hodograph transformation. $\Delta$ and $M$ stand for a forward difference operator and an average operator

$$\Delta F_k = \frac{F_{k+1} - F_k}{\delta_k}\,, \qquad MF_k = \frac{F_k + F_{k+1}}{2}\,,$$

respectively.

Equation (2) is also called a semi-discrete CH equation in [24]. It was shown that the equation (2) has the $N$-soliton solution which, in the continuous limit, approach the $N$-soliton solution of the CH equation including the $N$-cuspon solution. Therefore, the equation (2) is an integrable semi-discretization of the CH equation. The $N$-soliton solution is of the form

$$w_k = \left(\log \frac{g_k}{h_k}\right)_t\,, \tag{3}$$

with

$$f_k = \tau_0(k)\,, \qquad g_k = \tau_1(k)\,, \qquad h_k = \tau_{-1}(k)\,,$$

$$\tau_n(k) = \begin{vmatrix} \psi_1^{(n)} & \psi_1^{(n+1)} & \cdots & \psi_1^{(n+N-1)} \\ \psi_2^{(n)} & \psi_2^{(n+1)} & \cdots & \psi_2^{(n+N-1)} \\ \vdots & \vdots & & \vdots \\ \psi_N^{(n)} & \psi_N^{(n+1)} & \cdots & \psi_N^{(n+N-1)} \end{vmatrix}$$

where

$$\psi_i^{(n)} = a_{i,1}(p_i - c)^n(1 - ap_i)^{-k}e^{\xi_i} + a_{i,2}(-p_i - c)^n(1 + ap_i)^{-k}e^{\eta_i}\,,$$

$$\xi_i = \frac{1}{p_i - c} t + \frac{1}{(p_i - c)^2} s + \xi_{i0}\,,$$
$$\eta_i = -\frac{1}{p_i + c} t + \frac{1}{(p_i + c)^2} s + \eta_{i0}\,,$$
$$c = \frac{1}{\kappa}.$$

See [24] for the detailed proof.

Next, let us show that in the continuous limit, $a \to 0$ ($\delta_k \to 0$), the proposed scheme is consistent with the CH equation. To this end, the equation (2) is rewritten as

$$\begin{cases} \dfrac{-2}{\delta_k + \delta_{k-1}} (\Delta w_k - \Delta w_{k-1}) + \dfrac{\delta_k M w_k}{\delta_k + \delta_{k-1}} + \dfrac{\delta_{k-1} M w_{k-1}}{\delta_k + \delta_{k-1}} + \dfrac{1}{c(1 - a^2 c^2)} \\ \qquad\qquad = \dfrac{4a^2 c}{1 - a^2 c^2} \dfrac{1}{\delta_k \delta_{k-1}}\,, \\ \partial_t \delta_k = \left(1 - \dfrac{\delta_k^2}{4}\right) (w_{k+1} - w_k)\,. \end{cases}$$

By taking logarithmic derivative of the first equation, we get

$$\begin{cases} \dfrac{\partial_t \left\{ \dfrac{2}{\delta_k + \delta_{k-1}} (\Delta w_k - \Delta w_{k-1}) - \dfrac{\delta_k M w_k}{\delta_k + \delta_{k-1}} - \dfrac{\delta_{k-1} M w_{k-1}}{\delta_k + \delta_{k-1}} \right\}}{\dfrac{2}{\delta_k + \delta_{k-1}} (\Delta w_k - \Delta w_{k-1}) - \dfrac{\delta_k M w_k}{\delta_k + \delta_{k-1}} - \dfrac{\delta_{k-1} M w_{k-1}}{\delta_k + \delta_{k-1}} - \dfrac{1}{c(1 - a^2 c^2)}} \\ \qquad\qquad = -\dfrac{\partial_t \delta_k}{\delta_k} - \dfrac{\partial_t \delta_{k-1}}{\delta_{k-1}}\,, \\ \partial_t \delta_k = \left(1 - \dfrac{\delta_k^2}{4}\right) (w_{k+1} - w_k)\,. \end{cases}$$

Thus, we have

$$\frac{\partial_t \left\{ \dfrac{2}{\delta_k + \delta_{k-1}} (\Delta w_k - \Delta w_{k-1}) - \dfrac{\delta_k M w_k}{\delta_k + \delta_{k-1}} - \dfrac{\delta_{k-1} M w_{k-1}}{\delta_k + \delta_{k-1}} \right\}}{\dfrac{2}{\delta_k + \delta_{k-1}} (\Delta w_k - \Delta w_{k-1}) - \dfrac{\delta_k M w_k}{\delta_k + \delta_{k-1}} - \dfrac{\delta_{k-1} M w_{k-1}}{\delta_k + \delta_{k-1}} - \dfrac{1}{c(1 - a^2 c^2)}}$$
$$= -\left(1 - \frac{\delta_k^2}{4}\right) \Delta w_k - \left(1 - \frac{\delta_{k-1}^2}{4}\right) \Delta w_{k-1}\,.$$

The dependent variable $w$ is a function of $k$ and $t$, and we regard them as a function of $X$ and $T$, where $X$ is the space coordinate of the $k$-th lattice point and $T$ is the time, defined by

$$X = X_0 + \sum_{j=0}^{k-1} \delta_j \,, \qquad T = t \,.$$

Then in the continuous limit, $a \to 0$ ($\delta_k \to 0$), we have

$$\frac{w_{k+1} - w_k}{\delta_k} \to \frac{\partial w}{\partial X} \,, \qquad \frac{w_{k+1} + w_k}{2} \to w \,,$$

$$\frac{\partial X}{\partial t} = \frac{\partial X_0}{\partial t} + \sum_{j=0}^{k-1} \frac{\partial \delta_j}{\partial t} = \frac{\partial X_0}{\partial t} + \sum_{j=0}^{k-1} \left(1 - \frac{\delta_j^2}{4}\right)(w_{j+1} - w_j) \to w \,,$$

$$\partial_t = \partial_T + \frac{\partial X}{\partial t}\partial_X \to \partial_T + w\partial_X \,,$$

where the origin of space coordinate $X_0$ is taken so that $\dfrac{\partial X_0}{\partial t}$ cancels $w_0$. Then the above semi-discrete CH equation converges to the CH equation

$$\frac{(\partial_T + w\partial_X)(w_{XX} - w)}{w_{XX} - w - \dfrac{1}{c}} = -2w_X \,,$$

i.e.

$$(\partial_T + w\partial_X)(w_{XX} - w) = -2w_X \left(w_{XX} - w - \frac{1}{c}\right) . \tag{4}$$

Setting $c = 1/\kappa$, $w = u/\kappa$, $T = \kappa\tilde{T}$, we obtain the standard form of the CH equation

$$u_{\tilde{T}} + 2\kappa^2 u_X - u_{\tilde{T}XX} + 3uu_X = 2u_X u_{XX} + uu_{XXX}. \tag{5}$$

## 3. Implementation of the self-adaptive mesh method

First, we discuss how to implement the self-adaptive method in actual computations. Generally, given an arbitrary initial condition $w(X, 0) = w_0(X)$, the initial non-uniform mesh $\delta_k$ can be obtained by solving the nonlinear algebraic equations by Newton's iteration method. However, for the propagation or interaction of solitons or cuspons, which are challenging problems numerically, the

initial condition $w_k$ can be calculated by (3) from $g_k$ and $h_k$ by putting $t = 0$, which are obtainable from the corresponding determinant solutions. The initial non-uniform mesh $\delta_k$ can also be calculated by [24]

$$\delta_k = 2\frac{(1+ac)g_{k+1}h_k - (1-ac)g_k h_{k+1}}{(1+ac)g_{k+1}h_k + (1-ac)g_k h_{k+1}}. \tag{6}$$

On the other hand, once the non-uniform mesh $\delta_k$ is known, the solution $w_k$ can be easily obtained by solving a tridiagonal linear system based on the first equation of the scheme.

$$a_l w_{l-1}^{n+1} + b_l w_l^{n+1} + c_l w_{l+1}^{n+1} = d_l, \tag{7}$$

where

$$a_l = 0.5\delta_{k-1}^{n+1} - \frac{2}{\delta_{k-1}^{n+1}};\ \ b_l = 0.5(\delta_{k-1}^{n+1} + \delta_k^{n+1}) + \frac{2}{\delta_{k-1}^{n+1}} + \frac{2}{\delta_k^{n+1}};\ \ c_l = 0.5\delta_k^{n+1} - \frac{2}{\delta_k^{n+1}};$$

and

$$d_l = \frac{4a^2c}{1-a^2c^2}\left(\frac{1}{\delta_k^{n+1}} + \frac{1}{\delta_{k-1}^{n+1}}\right) - \frac{\delta_{k-1}^{n+1} + \delta_k^{n+1}}{c(1-a^2c^2)}\,.$$

In regard to the evolution of $\delta_k$, we propose two time advancing methods. The first is the modified forward Euler method, where we assume $w_k$ remains unchanged in one time step. Integrating once, we have

$$\delta_k^{n+1} = 2\frac{c_k^n e^{(w_{k+1}^n - w_k^n)\Delta t} - 1}{c_k^n e^{(w_{k+1}^n - w_k^n)\Delta t} + 1}, \tag{8}$$

where $c_k^n = (2+\delta_k^n)/(2-\delta_k^n)$. The second is the classical 4th-order Runge-Kutta method, where $w_k$ can be viewed as a function of $\delta_k$ by solving the above tridiagonal linear system. Therefore, in one time step, we have to solve tridiagonal linear system four times.

In summary, the numerical computation in one time-step only involves a ODE solver for non-uniform mesh and a tridiagonal linear system solver. Hence, the computation cost is much less than other existing numerical methods. A Matlab code is made to perform all the computations. Iterative methods, for instance, the Bi-conjugate gradient method bicg in Matlab are used to solve the tridiagonal system.

Finally, we list exact one- and two- soliton/cuspon and peakon solutions for the use of numerical experiments in the subsequent section.

**(1). One soliton/cuspon solution**: The $\tau$-functions for the one soliton/cuspon solution are

$$g \propto 1 \pm \left(\frac{c-p_1}{c+p_1}\right) e^{\xi_1}\,, \qquad h \propto 1 \pm \left(\frac{c+p_1}{c-p_1}\right) e^{\xi_1}\,, \tag{9}$$

with $\xi_1 = p_1(2x - v_1 t - x_{10})$, $v_1 = 2/(c^2 - p_1^2)$. This leads to a solution

$$w(x,t) = \frac{2p_1^2 c v_1}{(c^2+p_1^2) \pm (c^2-p_1^2)\cosh\xi_1}\,, \tag{10}$$

$$X = 2cx + \log\left(\frac{g}{h}\right)\,, \quad T = t\,, \tag{11}$$

where the positive case in Eq.(10) stands for the one smooth soliton solution when $p_1 < c$, while the negative case in Eq.(10) stands for the one-cuspon solution when $p_1 > c$. Otherwise, the solution is singular. Thus Eq.(10) for nonsingular cases can be expressed by

$$w(x,t) = \frac{2p_1^2 c v_1}{(c^2+p_1^2) + |c^2-p_1^2|\cosh\xi_1}\,. \tag{12}$$

Similarly, for the semi-discrete case, we have

$$g_k \propto 1 + \left|\frac{c-p_1}{c+p_1}\right| \left(\frac{1+ap_1}{1-ap_1}\right)^k e^{\xi_1}\,, \qquad h_k \propto 1 + \left|\frac{c+p_1}{c-p_1}\right| \left(\frac{1+ap_1}{1-ap_1}\right)^k e^{\xi_1}\,, \tag{13}$$

with $\xi_1 = p_1(-v_1 t - x_{10})$, resulting a solution of the form

$$w_k(t) = \frac{2p_1^2 c v_1}{(c^2+p_1^2) + |c^2-p_1^2| \left[\left(\left(\frac{1+ap_1}{1-ap_1}\right)^{-k} e^{-\xi_1} + \left(\frac{1+ap_1}{1-ap_1}\right)^{k} e^{\xi_1}\right)/2\right]}, \tag{14}$$

in conjunction with a transform between an uniform mesh ("$a$") and a non-uniform mesh

$$\delta_k = 2\frac{(1+ac)g_{k+1}h_k - (1-ac)g_k h_{k+1}}{(1+ac)g_{k+1}h_k + (1-ac)g_k h_{k+1}}. \tag{15}$$

Equation (14) corresponds to the 1-soliton solution when $p < c$, the 1-cuspon solution when $p > c$.

**(2). Two soliton/cuspon solutions**: The $\tau$-functions for the two soliton/cuspon solution are

$$g \propto 1 + \left|\frac{c_1-p_1}{c_1+p_1}\right| e^{\xi_1} + \left|\frac{c_2-p_2}{c_2+p_2}\right| e^{\xi_2} + \left|\frac{(c_1-p_1)(c_2-p_2)}{(c_1+p_1)(c_2+p_2)}\right| \left(\frac{p_1-p_2}{p_1+p_2}\right)^2 e^{\xi_1+\xi_2}\,,$$

$$h \propto 1 + \left|\frac{c_1+p_1}{c_1-p_1}\right| e^{\xi_1} + \left|\frac{c_2+p_2}{c_2-p_2}\right| e^{\xi_2} + \left|\frac{(c_1+p_1)(c_2+p_2)}{(c_1-p_1)(c_2-p_2)}\right| \left(\frac{p_1-p_2}{p_1+p_2}\right)^2 e^{\xi_1+\xi_2},$$

with $\xi_1 = p_1(2x - v_1 t - x_{10})$, $\xi_2 = p_2(2x - v_2 t - x_{20})$, $v_1 = 2/(c_1^2 - p_1^2)$, $v_2 = 2/(c_2^2 - p_2^2)$. The parametric solution can be calculated through

$$w(x,t) = \left(\log \frac{g}{h}\right)_t, \qquad X = 2cx + \log\left(\frac{g}{h}\right), \quad T = t, \tag{16}$$

whose form is complicated and is omitted here. Note that the above expression includes the two-soliton solution ($p_1 < c_1$, $p_2 < c_2$), the two-cuspon solution ($p_1 > c_1$, $p_2 > c_2$), or the soliton-cuspon solution ($p_1 < c_1$, $p_2 > c_2$).

Similarly, for the semi-discrete case, we have

$$\begin{aligned} g_k \propto 1 &+ \left|\frac{c_1-p_1}{c_1+p_1}\right| \left(\frac{1+ap_1}{1-ap_1}\right)^k e^{\xi_1} + \left|\frac{c_2-p_2}{c_2+p_2}\right| \left(\frac{1+ap_2}{1-ap_2}\right)^k e^{\xi_2} \\ &+ \left|\frac{(c_1-p_1)(c_2-p_2)}{(c_1+p_1)(c_2+p_2)}\right| \left(\frac{p_1-p_2}{p_1+p_2}\right)^2 \left(\frac{1+ap_1}{1-ap_1}\right)^k \left(\frac{1+ap_2}{1-ap_2}\right)^k e^{\xi_1+\xi_2}, \end{aligned}$$

$$\begin{aligned} h_k \propto 1 &+ \left|\frac{c_1+p_1}{c_1-p_1}\right| \left(\frac{1+ap_1}{1-ap_1}\right)^k e^{\xi_1} + \left|\frac{c_2+p_2}{c_2-p_2}\right| \left(\frac{1+ap_2}{1-ap_2}\right)^k e^{\xi_2} \\ &+ \left|\frac{(c_1+p_1)(c_2+p_2)}{(c_1-p_1)(c_2-p_2)}\right| \left(\frac{p_1-p_2}{p_1+p_2}\right)^2 \left(\frac{1+ap_1}{1-ap_1}\right)^k \left(\frac{1+ap_2}{1-ap_2}\right)^k e^{\xi_1+\xi_2}, \end{aligned}$$

with $\xi_1 = p_1(-v_1 t - x_{10})$, $\xi_2 = p_2(-v_2 t - x_{20})$. The solution can be calculated through

$$w(x,t) = \left(\log \frac{g_k}{h_k}\right)_t, \tag{17}$$

with a transform

$$\delta_k = 2\frac{(1+ac)g_{k+1}h_k - (1-ac)g_k h_{k+1}}{(1+ac)g_{k+1}h_k + (1-ac)g_k h_{k+1}}. \tag{18}$$

Again, the explicit form of the solution is complicated and is omitted here.

**(3). Peakon solutions**:

In the continuous CH equation, it is possible to construct peakon solutions from soliton solutions by taking the peakon limit [3, 33, 4, 6, 8, 34, 35].

For the continuous case, we can express the 1-soliton solution as

$$w = \frac{2p_1^2\kappa v_1}{1 + p_1^2\kappa^2 + (1 - p_1^2\kappa^2)\cosh\xi_1},$$

where $\kappa = \frac{1}{c}$, $v_1 = 2\kappa^2/(1-p_1^2\kappa^2)$, $\xi_1 = p_1\kappa(2x/\kappa-(v_1/\kappa)t-x_{10}/\kappa)$. Taking the peakon limit $\kappa \to 0$, $p_1\kappa \to 1$, $v_1 = \text{const.}$, the solution $(X(x,t), w(x,t))$, where $X(x,t) = 2x/\kappa + \log\frac{g}{h}$, gives the 1-peakon solution [35]. In Fig.1, one can see that the 1-soliton solution approaches to the 1-peakon solution as $\kappa$ approaches to 0.

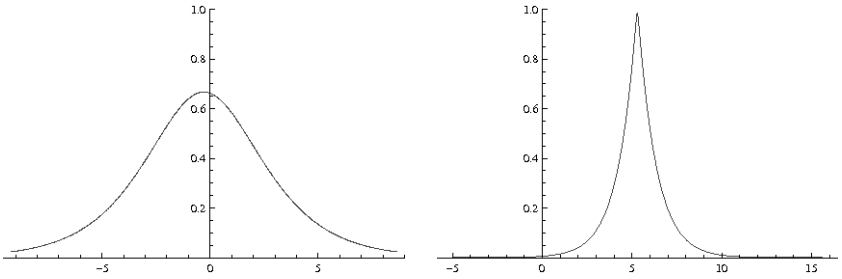


Figure 1: 1-soliton solution for the CH equation: the left: $p_1 = 0.5, c = 1$; the right (close to the peakon limit): $p_1 = 99, c = 100$.

We can also consider the peakon limit for the semi-discrete CH equation. For the semi-discrete case, we can express the 1-soliton solution as

$$w_k = \frac{2p_1^2\kappa v_1}{1 + p_1^2\kappa^2 + (1 - p_1^2\kappa^2)\left[\left(\left(\frac{1+ap_1}{1-ap_1}\right)^{-k} e^{-\xi_1} + \left(\frac{1+ap_1}{1-ap_1}\right)^{k} e^{\xi_1}\right)/2\right]},$$

where $\kappa = \frac{1}{c}$, $v_1 = 2\kappa^2/(1 - p_1^2\kappa^2)$, $\xi_1 = p_1\kappa(-(v_1/\kappa)t - x_{10}/\kappa)$. The peakon limit for the semi-discrete CH equation is again $\kappa \to 0$, $p_1\kappa \to 1$, $v_1 = \text{const}$. Taking the peakon limit, we expect that the solution $(X_k(t), w_k(t))$, where $X_k(t) = X_0 + \sum_{j=0}^{k-1}\delta_j(t)$, gives the 1-peakon solution. In Fig.2, one can see that the 1-soliton solution approaches to the 1-peakon solution as $\kappa$ approaches to 0.

From the above observation, we expect that there is an explicit form of the peakon solution for the semi-discrete CH equation. The detail of the peakon solution for the semi-discrete CH equation will be reported in the forthcoming paper.

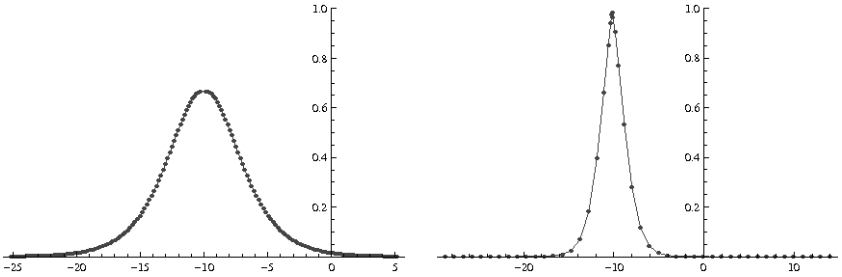


Figure 2: 1-soliton solution for the semi-discrete CH equation: the left: $p_1 = 0.5, c = 1, a = 0.1$; the right (close to the peakon limit): $p_1 = 99, c = 100, a = 0.005$.

## 4. Numerical experiments

In this section, we apply our scheme to several test problems. They include: 1) propagation and interaction of nearly-peakon solutions; 2) propagation and interaction of cuspon solutions; 3) interactions of soliton-cuspon solutions; 4) non-exact initial value problems.

### *4.1. Propagation and interaction of nearly-peakon solutions*

**Example 1: One peakon propagation.** It has been shown in [34, 35] that the analytic $N$-soliton solution of the CH equation converges to the nonanalytic $N$-peakon solution when $\kappa \to 0$ ($c \to \infty$). To show this, we choose one soliton solution with parameters $c = 1000$, $p = 998.9995$. Thus the speed of the soliton ($v_1/2$) is $1.0$. Its profile is plotted and is compared with one peakon solution $u(x,t) = e^{-|x-t|}$ in Fig.3. These two solutions are indistinguishable from the graph. The error in $L_\infty$, where $L_\infty = \max|w_l - u_l|$, is calculated to be $0.002$, and the discrepancy for the first conserved quantity $I_1 = \int u\,dx$ is less than $0.7\%$. Therefore, this soliton solution can be viewed as an approximate peakon solution with amplitude $1.0$.

The propagation of the above designed approximate peakon solution is solved by the self-adaptive mesh scheme with two different time advancing methods: the modified forward Euler method (MFE) and the classical Runge-Kutta method (RK4). The computation domain is about $28.5$. Figures 4 (a)-(d) display the numerical solutions at $t = 1.0, 2.0, 3.0, 4.0$, together with the self-adjusted mesh. It can be seen that the non-uniform mesh is dense around the crest. The most dense part of the non-uniform mesh moves along with the peakon point with the same speed. The errors in the $L_\infty$-norm and the first conserved quantity $I_1 = \int w\,dx$ are computed and compared in Table 1. Here, $L_\infty = \max|\tilde{w}_l - w_l|$, where $\tilde{w}_l$ and $w_l$

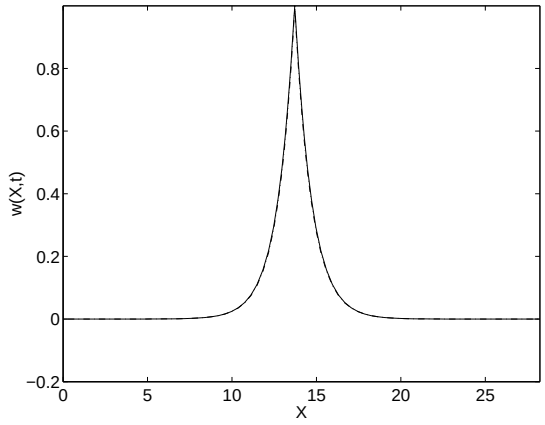


Figure 3: Comparison between one peakon solution and one-soliton solution with $c = 200.0$.

represent the numerical and analytical solutions at the grid points $X_l$, respectively. Here, $E_1 = |\bar{I}_1 - I_1|/|I_1|$ indicates the relative error, $\bar{I}_1$ stands for the counterpart of $I_1$ by the numerical solution. Trapezoidal rule on the non-uniform mesh is employed for the evaluation of the integrals.

**Example 2: Two peakon interaction.** For $c = 1000$, we initially choose two approximate peakon solutions moving with velocity $v_1/2 = 2.0$, and $v_2/2 = 1.0$, respectively. Their interaction is numerically solved by MFE and RK4, respectively, with a fixed grid number of $N = 101$. Figure 5 displays the process of collision at different times. Table 2 presents the errors in $L_\infty$-norm and $E_1$. It could be seen that, in spite of a small number of grid points and a large time step, RK4 simulates the collision of two approximate peakons with an amazing accuracy.

In regard to the propagation and interaction of approximate peakon solutions, we summarize as follows:

1. Due to the integrability of the scheme and the self-adaptive feature of the non-uniform mesh, the $L_\infty$-norm is small and the first conserved quantity is preserved extremely well even for a small number of grid points. Almost doubling the grid numbers from $51$ to $101$ doesn't get the accuracy improved since a grid number of $51$ is already good enough for the spatial resolution.
2. The errors is mainly due to the time advancing methods. FE1 is first order in time, so it produces relatively large $L_\infty$ and $E_1$, roughly changing in proportional with time. RK4 is fourth-order in time, so up to $T = 4.0$, $L_\infty$ and $E_1$

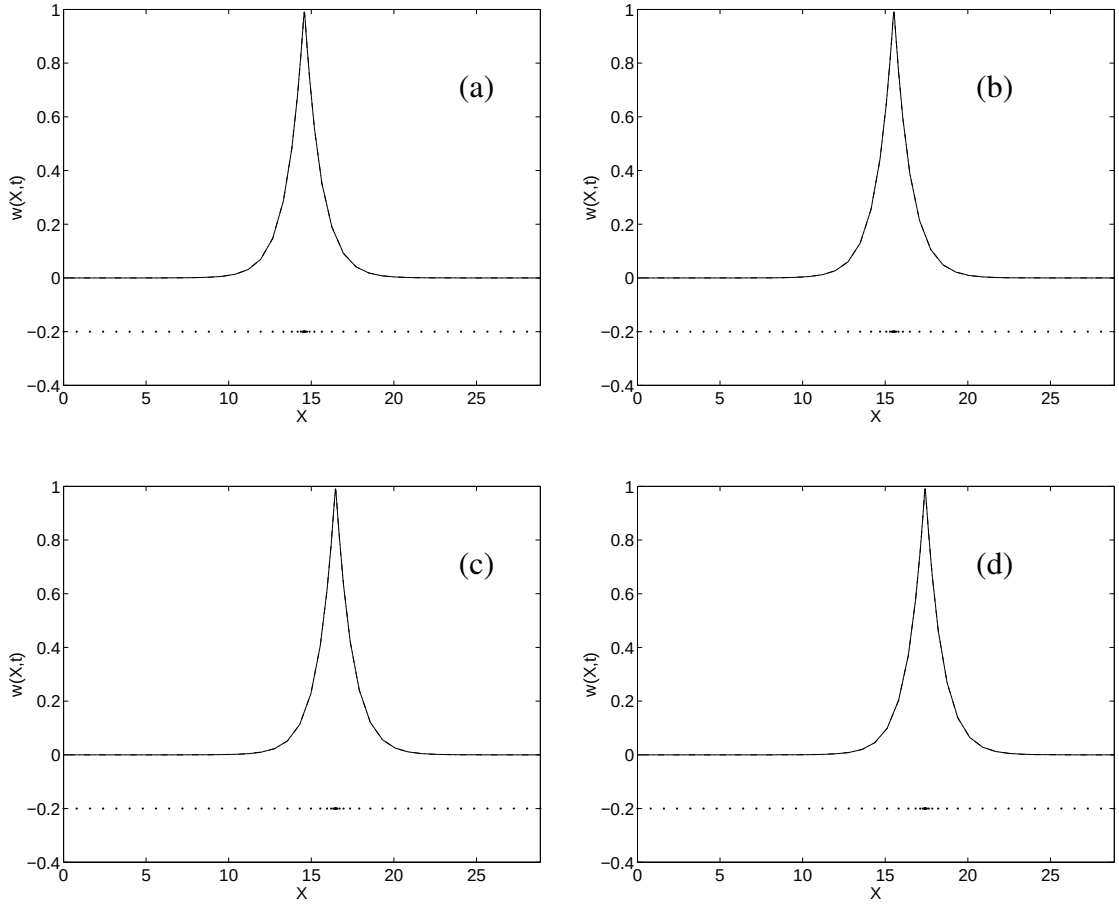


Figure 4: Numerical solution of one single peakon solution: (a) $t = 1.0$; (b) $t = 2.0$; (c) $t = 3.0$; (c) $t = 4.0$.

Table 1: Comparison of $L_\infty$ and $I_1$ errors by the self-adaptive mesh method

| T | N | $\Delta t$ | MFE | | RK4 | |
|---|---|---|---|---|---|---|
| | | | $L_\infty$ | $E_1$ | $L_\infty$ | $E_1$ |
| 2.0 | 51 | 0.01 | $6.6(-3)$ | $7.6(-3)$ | $8.5(-10)$ | $5.6(-8)$ |
| 4.0 | 51 | 0.01 | $1.5(-2)$ | $1.5(-2)$ | $9.0(-9)$ | $1.5(-6)$ |
| 2.0 | 51 | 0.05 | $3.4(-2)$ | $3.9(-2)$ | $8.4(-9)$ | $9.2(-10)$ |
| 4.0 | 51 | 0.05 | $7.9(-2)$ | $8.4(-2)$ | $1.5(-8)$ | $1.5(-6)$ |
| 2.0 | 101 | 0.01 | $6.8(-3)$ | $7.6(-3)$ | $5.6(-9)$ | $3.3(-7)$ |
| 4.0 | 101 | 0.01 | $1.5(-2)$ | $1.5(-2)$ | $5.4(-8)$ | $3.8(-6)$ |
| 2.0 | 101 | 0.05 | $3.5(-2)$ | $3.8(-2)$ | $9.4(-9)$ | $3.3(-7)$ |
| 4.0 | 101 | 0.05 | $8.2(-2)$ | $8.3(-2)$ | $5.4(-8)$ | $3.8(-6)$ |

Table 2: $L_\infty$ and $I_1$ errors for two approximate peakon interaction by the self-adaptive mesh method

| | $\Delta t$ | T | $L_\infty$ | $E_1$ |
|---|---|---|---|---|
| MFE | 0.001 | 5.0 | $2.2(-2)$ | $5.5(-3)$ |
| | 0.001 | 10.0 | $7.1(-2)$ | $1.2(-2)$ |
| RK4 | 0.05 | 5.0 | $6.6(-7)$ | $4.1(-7)$ |
| | 0.05 | 10.0 | $1.8(-7)$ | $1.4(-5)$ |
| | 0.01 | 5.0 | $2.0(-9)$ | $1.5(-7)$ |
| | 0.01 | 10.0 | $3.2(-9)$ | $1.4(-5)$ |

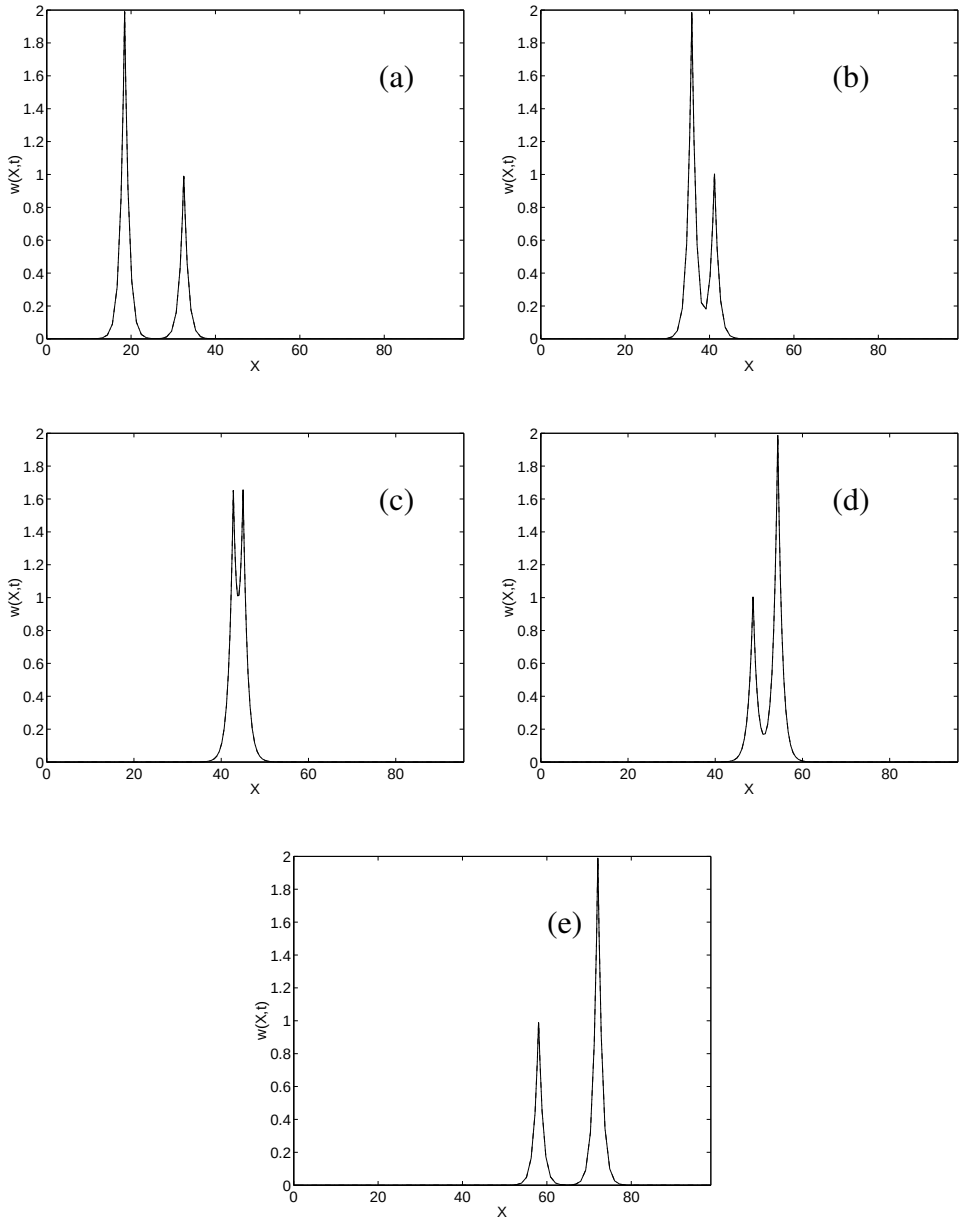


Figure 5: Numerical solution for collision of two nearly-peakon with $p_1 = 198.9975$, $p_2 = 199.4995$ and $c = 200.0$: (a) $t = 0.0$; (b) $t = 10.0$; (c) $t = 15.0$; (d) $t = 20.0$; (e) $t = 30.0$.

are of the orders $10^{-8}$ and $10^{-6}$ for a grid number of $N = 51$ and a time step $\Delta t = 0.05$.

*4.2. Propagation and interaction of cuspon solutions*

The classical 4th-order Runge-Kutta method fails whenever the cuspon solution is involved. It seems that a kind of instability occurs in this case, whose theoretical reason is still unclear. Therefore, only MFE is employed to conduct the numerical experiments hereafter.

**Example 3: One-cuspon propagation.** The parameters taken for the one-cuspon solution are $p = 10.98$, $c = 10.0$. The number of grid is taken as $101$ in an interval of width of $4$ in the $x$-domain. Through the hodograph transformation, this corresponds to an interval of width $74.34$ in the $X$-domain. Figure 6(a) shows the initial profile and the initial mesh. Figures 6(b)-(d) display the numerical solutions (solid line) and exact solutions (dotted line) at $t = 2, 3, 4$, together with the self-adjusted mesh. It can be seen that the non-uniform mesh is dense around the cuspon point, and moves to the left in accordance with the movement of the cuspon point. Table 3 exhibits the results of errors in $L_\infty$-norm and $E_1$.

Table 3: Errors in the $L_\infty$ norm and the first conservative quantity for the self-adaptive mesh method (2.1)

| $\Delta t$ | $t$ | $L_\infty$ | $E_1$ |
|---|---|---|---|
| $0.005$ | 2.0 | $3.3(-2)$ | $4.7(-2)$ |
| $0.005$ | 4.0 | $9.7(-2)$ | $1.2(-1)$ |
| $0.001$ | 2.0 | $1.1(-2)$ | $1.2(-2)$ |
| $0.001$ | 4.0 | $2.9(-2)$ | $3.7(-2)$ |

**Example 4: Two-cuspon interaction.** The parameters taken for the two-cuspon solutions are $p_1 = 11.0$, $p_2 = 10.5$, $c = 10.0$. Figures 7(a)-(d) display the process of collision at several different times, along with the exact solution. Meanwhile, the self-adaptive mesh is also shown in the graph. It can be seen that two cuspon solutions undertake elastic collision, regaining their shapes after the collision is complete. As mentioned in [10], the two cuspon points are always present during the collision. The grid points are automatically adapted with the movement of the cuspons, and are always concentrated at the cuspon points. In compared with the exact solutions, we can comment that the numerical solutions

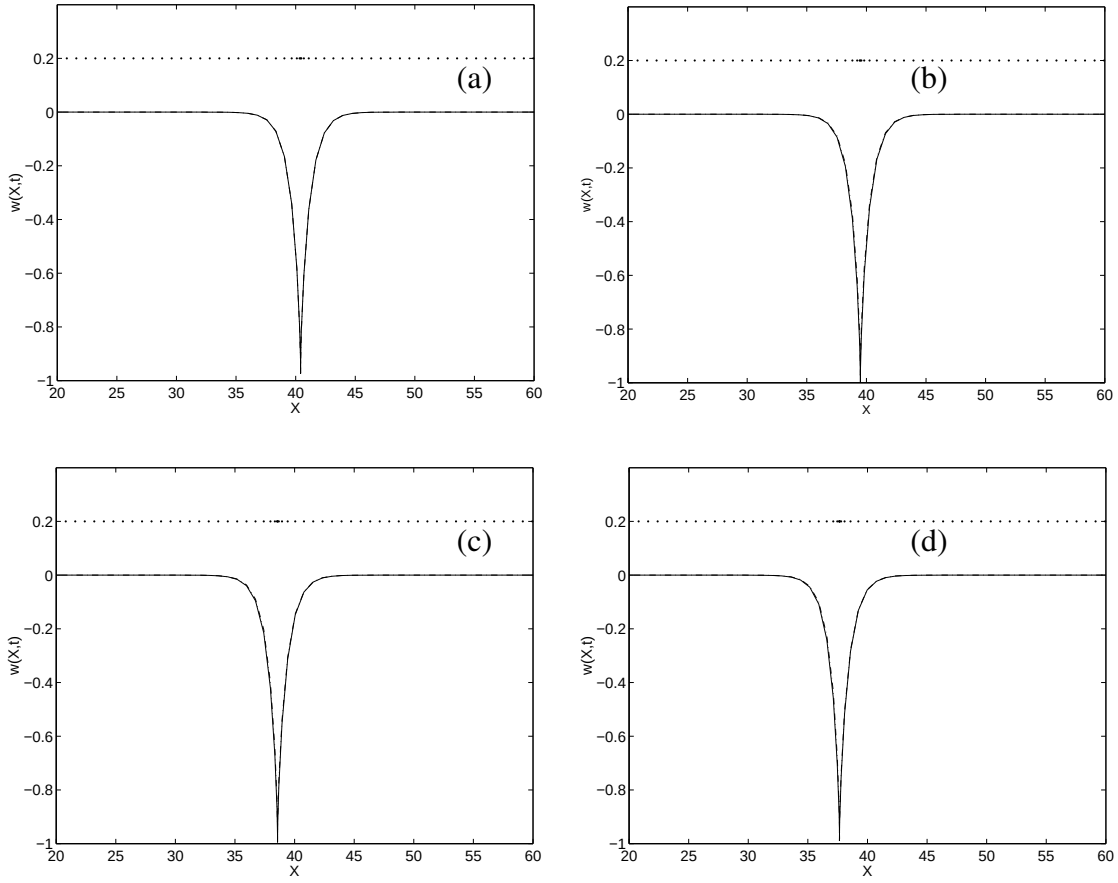


Figure 6: Numerical solution of one single cuspon solution: (a) $t = 0.0$; (b) $t = 2.0$; (c) $t = 3.0$; (c) $t = 4.0$.

are in a good agreement with exact solutions. As far as we know, what is shown here is the first numerical demonstration for the cuspon-cuspon interaction.

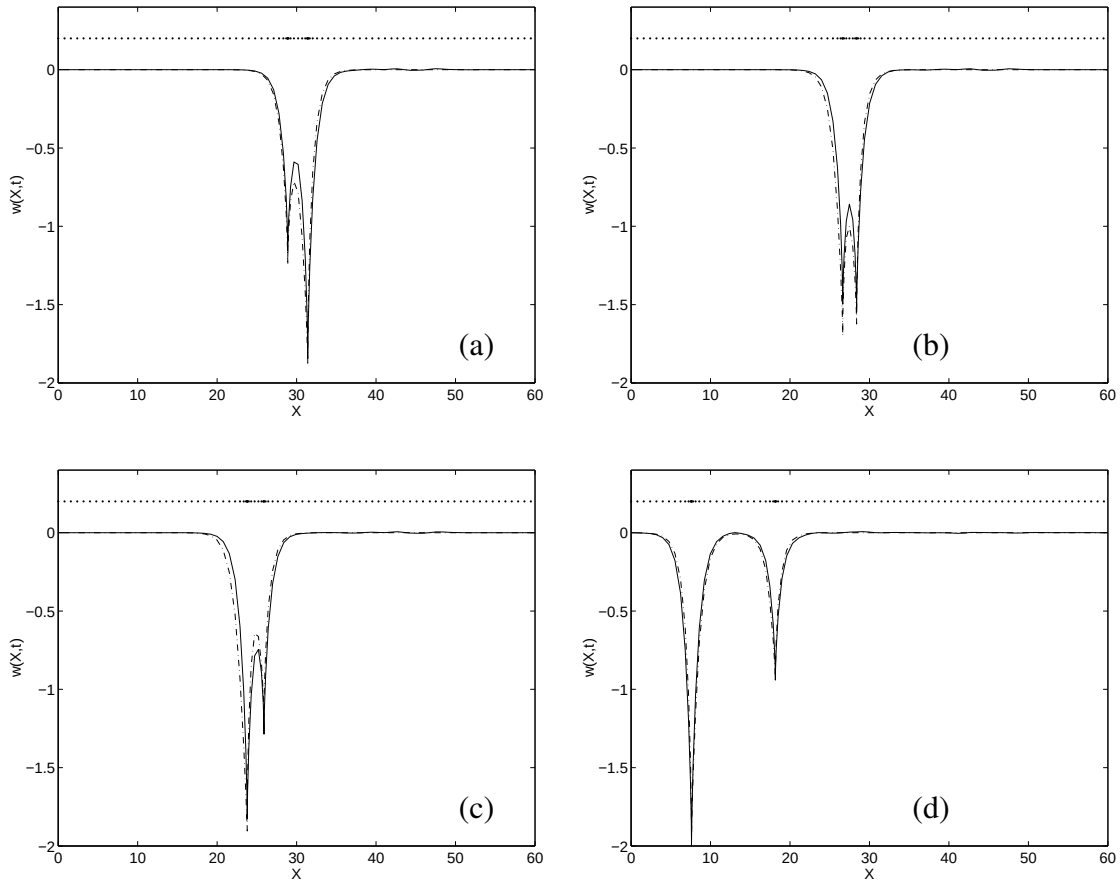


Figure 7: Numerical solution for the collision of two-cuspon solution with $p_1 = 11.0$, $p_2 = 10.5$, $c = 10.0$: (a) $t = 13.0$; (b) $t = 14.8$; (c) $t = 16.6$; (d) $t = 25.0$.

### *4.3. Soliton-cuspon interactions*

Here we show two examples for the soliton-cuspon interaction with $c = 10.0$. In Fig.8, we plot the interaction process between a soliton of $p_1 = 9.12$ and a cuspon of $p_2 = 10.98$ at several different times where the soliton and the cuspon have almost the same amplitude. It can be seen that when the collision starts ($t = 12.0$), another singularity point with infinite derivative ($w_x$) occurs. As collision goes on ($t = 14.4, 14.6, 14.8$), the soliton seems 'eats up' the cuspon,

and the profile looks like a complete elevation. However, the cuspon point exists at all times, especially, at $t = 14.6$, the profile becomes one symmetrical hump with a cuspon point in the middle of the hump.

In Fig.9, we present another example of a collision between a soliton ($p_1 = 9.12$) and a cuspon ($p_2 = 10.5$) where the cuspon has a larger amplitude (2.0) than the soliton (1.0). Again, when the collision starts, another singularity point appears. As collision goes on, the soliton is gradually absorbed by the cuspon. At $t = 10.3$, the whole profile looks like a single cuspon when the soliton is completely absorbed. Later on, the soliton reappears from the right until $t = 16$, the soliton and cuspon recover their original shapes except for a phase shift when the collision is complete.

*4.4. Non-exact initial value problems*

Here, we show that the integrable scheme can also be applied for the initial value problem starting with non exact solutions. To the end, we choose an initial condition whose mesh size is determined by

$$\delta_k = 2\,c\,h\,(1 - 0.8\,\mathrm{sech}(2kh - W_x/2)), \tag{19}$$

then, the initial profile can be calculated through the second equation of the semi-discretization, which is plotted in Fig.10 (a). Figures 10 (b), (c) and (d) show the evolutions at $t = 10, 20, 30$, respectively. Note that $c = 10$ in this computation. It can be seen that a soliton with large amplitude is firstly developed, and moving fast to the right. By $t = 30$, a second soliton with small amplitude is to be developed.

Next, we increase the value of $c$ to 90, which implies a very small dispersion term, corresponding to the dispersionless CH equation. The initial profile and the evolutions at $t = 50, 150, 200$ are shown in Fig.11. It is seen that four nearly-peakons are developed from the initial profile at $t = 50$. Later on, an array of nearly-peakons of seven and eight are developed at $t = 150, 200$, respectively. This result is similar to the result for the KdV type equations with a small dispersion, i.e. the peakon trains are generated. (For the KdV type equations, soliton trains are generated. For example, see [36, 37] for numerical simulations and [38] for a theoretical analysis for the KdV equation.) A theoretical analysis for the dispersionless CH equation to explain the above intriguing numerical result is called for.

## 5. Concluding Remarks

In the present paper, we have proposed a self-adaptive mesh method for the CH equation, which based on an integrable semi-discretization of the CH equa-

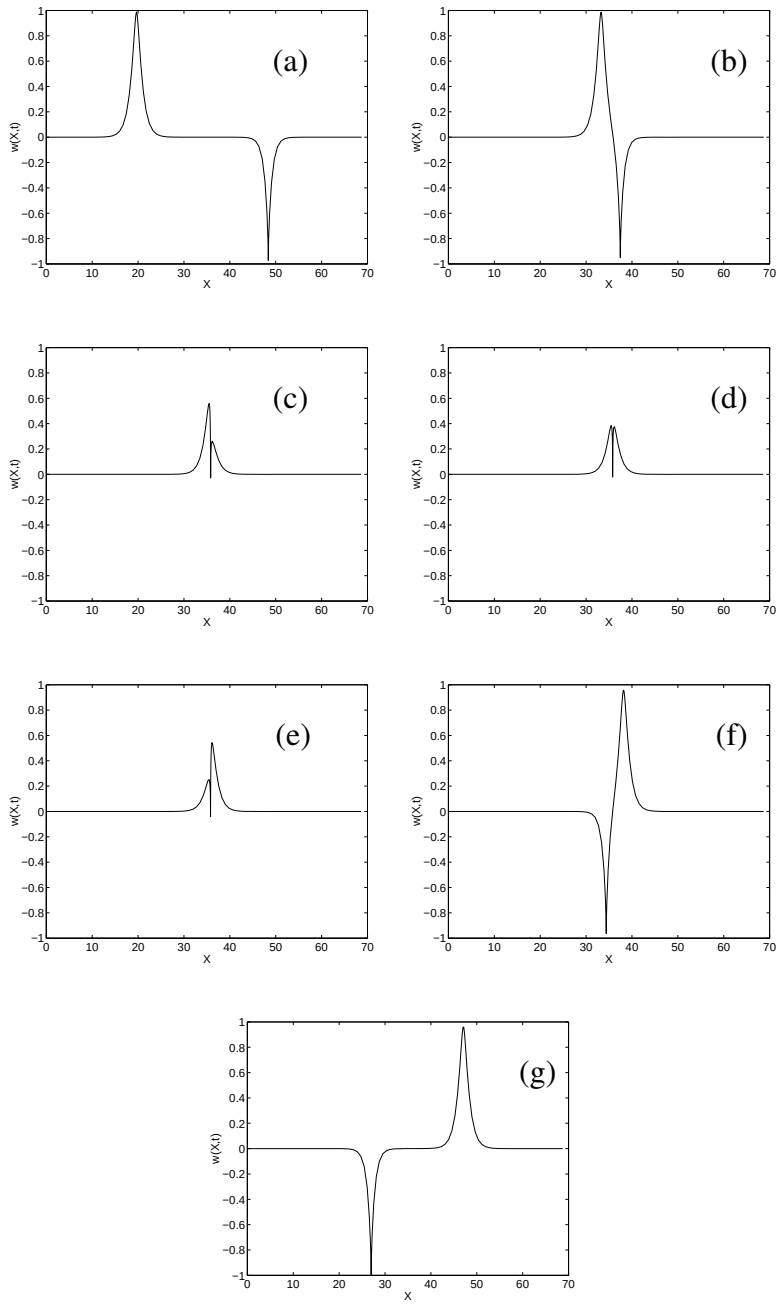


Figure 8: Numerical solution for cuspon-soliton collision with $p_1 = 9.12$, $p_2 = 10.98$ and $c = 10.0$: (a) $t = 0.0$; (b) $t = 12.0$; (c) $t = 14.4$; (d) $t = 14.6$; (e) $t = 14.8$; (f) $t = 17.0$; (g) $t = 25.0$.

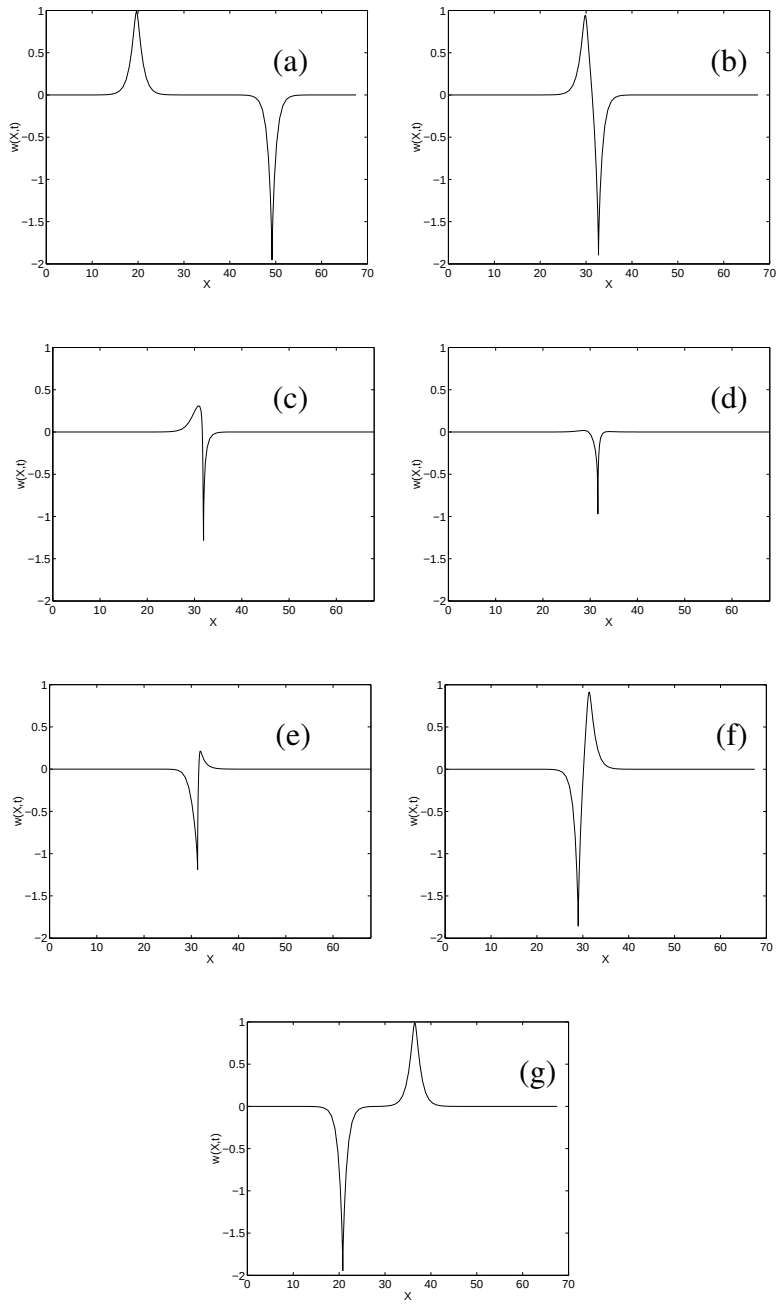


Figure 9: Numerical solution for cuspon-soliton collision with $p_1 = 9.12$, $p_2 = 10.5$ and $c = 10.0$: (a) $t = 0.0$; (b) $t = 9.0$; (c) $t = 10.0$; (d) $t = 10.3$; (e) $t = 10.6$; (f) $t = 11.5$; (g) $t = 16.0$.

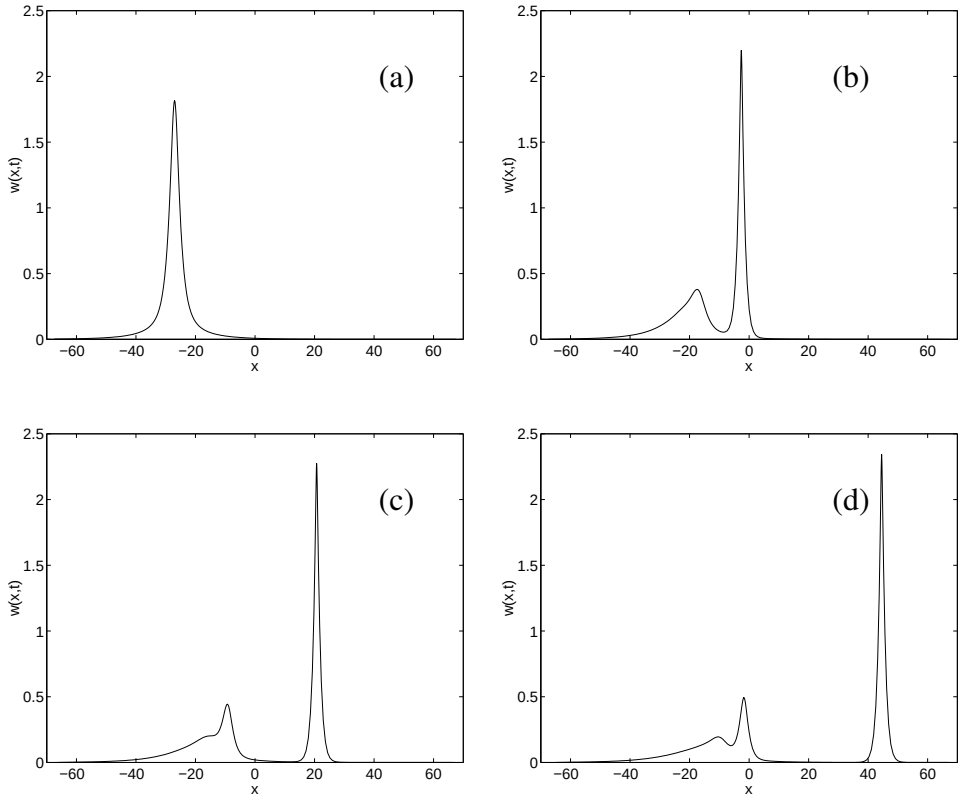


Figure 10: Numerical solution starting from an initial condition (19) with $c = 10$: (a) $t = 0.0$; (b) $t = 10.0$; (c) $t = 20.0$; (d) $t = 30.0$.

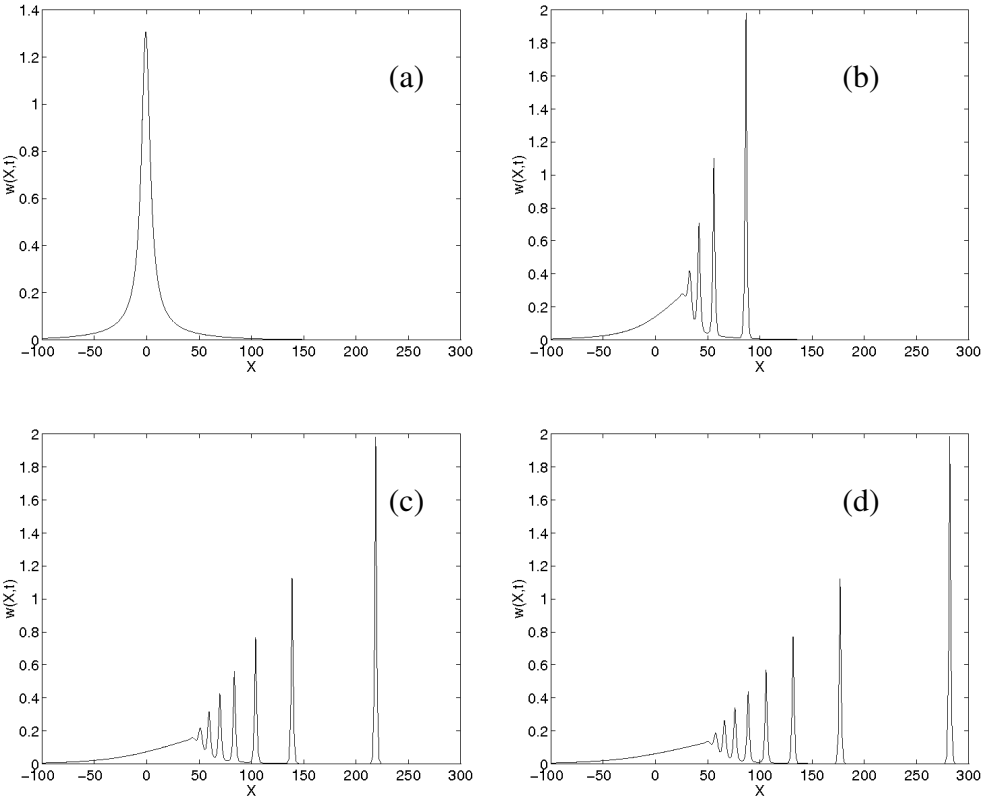


Figure 11: Numerical solution starting from an initial condition (19) with $c = 90$: (a) $t = 0.0$; (b) $t = 50.0$; (c) $t = 150.0$; (d) $t = 200.0$.

tion. It has the properties: (1) it is integrable in the sense that the scheme itself admits the $N$-soliton solution approaching to the $N$-soliton solution of the CH equation in the limit of mesh size going to zero; (2) the mesh is non-uniform and is automatically adjusted so that it is concentrated in the region where the solution changed sharply, for example, the cuspon point; (3) once the non-uniform mesh is evolved, the solution is determined from the evolved mesh by solving a tridiagonal linear system. Therefore, either from the accuracy or from the computation cost, the proposed method is expected to be superior than other existing numerical methods of the CH equation. This is indeed true. The numerical results in this paper indicate that a very good accuracy is obtained.

Two time advancing methods, the modified forward Euler method and the classical 4th-order Runge-Kutta method, are used to solve the evolution of non-uniform mesh. The Runge-Kutta method gains much better accuracy than the modified forward Euler method. However, it fails for the computations of cuspons. Using the self-adaptive mesh method for the CH equation, we have obtained interesting numerical computation results starting with non-exact solutions. When $\kappa$ is very small, the peakon train is generated from the non-exact initial condition.

As further topics, it is interesting to construct a self-adaptive mesh method to the Degasperis-Procesi (DP) equation [39]

$$u_T + 3\kappa^3 u_X - u_{TXX} + 4uu_X = 3u_X u_{XX} + uu_{XXX}. \tag{20}$$

The DP equation is also known as an integrable system sharing some common features with the CH equation, for example, the existence of $N$-soliton solutions through hodograph transformations [40, 41]. It is possible to construct an integrable semi-discrete DP equation by using the same approach, which implies a self-adaptive mesh method for the numerical simulations. We will report the related results in the near future.

**Acknowledgments**

B.F. is grateful for the support of the U.S. Army Research Office under Contract No. W911NF-05-1-0029. Y.O. and K.M. are grateful for the hospitality of the Isaac Newton Institute for Mathematical Sciences (INI) in Cambridge where this article was completed during the programme Discrete Integrable Systems (DIS).

## References


[1] R. Camassa and D. Holm, An integrable shallow water equation with peaked solitons, Phys. Rev. Lett. **71**, 1661 (1993).

[2] B. Fuchssteiner and A. Fokas, Symplectic structures, their Bäcklund transformations and hereditary symmetries, Physica D **4**, 47 (1981).

[3] R. Camassa, D.D. Holm, and J.M. Hyman, A new integrable shallow water equation, Adv. Appl. Mech. **31**, 1 (1994).

[4] J. Schiff, The Camassa-Holm equation: A loop group approach, Physica D **121** (1998) 24.

[5] M. C. Ferreira, R. A. Kraenkel, and A. I. Zenchuk, Soliton-cuspon interaction for the Camassa-Holm equation, J. Phys. A: Math. Gen., **32**, 8665(1999).

[6] R.S. Johnson, On solutions of the Camassa-Holm equation, Proc. R. Soc. London **A459**, 1687 (2003).

[7] Y. Li and J.E. Zhang, The multiple-soliton solution of the Camassa-Holm equation, Proc. R. Soc. London **A460** (2004) 2617.

[8] A. Parker, On the Camassa-Holm equation and a direct method of solution. I. Bilinear form and solitary waves, Proc. R. Soc. London **A460**, 2929 (2004).

[9] A. Parker, On the Camassa-Holm equation and a direct method of solution. II. Soliton solutions, Proc. R. Soc. London **A461**, 3611 (2005).

[10] H.-H. Dai and Y. Li, The interaction of the $\omega$-soliton and the $\omega$-cuspon of the Camassa-Holm equation, J. Phys. A: Math. Gen. **38** (2005) L685.

[11] Y. Matsuno, Parametric Representation for the Multisoliton Solution of the Camassa-Holm Equation, J. Phys. Soc. Japan, **74**, (2005) 1983.

[12] H. Kalisch and J. Lenells, Numerical study of traveling-wave solutions for the Camassa-Holm equation, Chaos, Solitons & Fractals, **25**, 287 (2005).

[13] H. Holden and X. Raynaud, Convergence of a Finite Difference Scheme for the Camassa-Holm Equation, SIAM J. Numer. Anal., **44**, 1655 (2006).

[14] G. M. Coclite, K. H. Karlsen, and N. H. Risebro, A Convergent Finite Difference Scheme for the Camassa-Holm Equation with General $H^1$ Initial Data, SIAM J. Numer. Anal., **46**, 1554(2008).

[15] R. Artebrant and H. J. Schroll, Numerical simulation of Camassa-Holm peakons by adaptive upwinding, Appl. Numer. Math., **56**, 695 (2006).

[16] Y. Xu and C.-W. Shu, A local discontinuous Galerkin method for the Camassa-Holm equation, SIAM J. Numer. Anal., **46**, 1998 (2008).

[17] T. Matsuo and H. Yamaguchi, An energy-conserving Galerkin scheme for a class of nonlinear dispersive equations, J. Comput. Phys., **228**, 4346 (2009).

[18] D.Cohen, B. Owren, and X. Raynaud, Multi-symplectic integration of the Camassa-Holm equation, J. Comput. Phys., **227**, 5492 (2008).

[19] R. Camassa, Characteristics and the initial value problem of a completely integrable shallow water equation, Discrete Cont. Dyn.-B, **3**, 115(2003).

[20] R. Camassa, J. Huang, and L. Lee, On a completely integrable numerical scheme for a nonlinear shallow-water wave equation, J. Nonlinear Math. Phys., **12**, 146 (2005).

[21] R. Camassa, J. Huang, and L. Lee, Integral and integrable algorithms for a nonlinear shallow-water wave equation, J. Comput. Phys., **216**, 547 (2006).

[22] R. Camassa and L. Lee, Complete integrable particle methods and the recurrence of initial states for a nonlinear shallow-water wave equation, J. Comput. Phys., **227**, 7206 (2008).

[23] H. Holden and X. Raynaud, A convergent numerical scheme for the Camassa-Holm equation based on multipeakons, Discrete Contin. Dyn. Syst., **14**, 505 (2006).

[24] Y. Ohta, K. Maruno, and B. F. Feng, An integrable semi-discretization of the Camassa-Holm equation and its determinant solution, J. Phys. A **41**, 355205 (2008).

[25] A. Harten and J.M. Hyman, Self-adjusting grid methods for one-dimensional hyperbolic conservation laws, J. Comput. Phys. **50**, 235 (1983).

[26] K. Miller and R. N. Miller, Moving finite elements.I, SIAM J. Numer. Anal. **18**, 1019 (1981).

[27] E. A. Dorfi and T. J. Kaper, Simple adaptive grids for 1-d initial value problems, J. Comput. Phys. **69**, 175 (1987).

[28] J. U. Brackbill, An adaptive grid with directional control, J. Comput. Phys. **108**, 38 (1993).

[29] W. M. Cao, W. Z. Huang, and R. D. Russell, An r-adaptive finite element method based upon moving mesh PDEs, J. Comput. Phys. **149**, 221(1999).

[30] J. M. Stockie, J. A. Mackenzie, and R. D. Russell, A moving mesh method for onedimensional hyperbolic conservation laws, SIAM J. Sci. Comput. **22**, 1791 (2001).

[31] H. Z. Tang and and T. Tang, Adaptive mesh methods for one- and two-dimensional hyperbolic conservation laws, SIAM J. Numer. Anal. **41**, 487(2003).

[32] R. Fazio and R. J. LeVeque, Moving-Mesh Methods for One-Dimensional Hyperbolic Problems Using CLAWPACK, Computers and Mathematics with Applications **45**, 273 (2003).

[33] Y. Li and P. Olver, Convergence of solitary wave solutions in a perturbed bi-Hamiltonian dynamical system. I. Compactons and peakons, Discrete Contin. Dynam. Syst. A, **3** (1997) 419.

[34] A. Parker and Y. Matsuno, The Peakon Limits of Soliton Solutions of the Camassa-Holm Equation, J. Phys. Soc. Japan, **75** (2006) 124001.

[35] Y. Matsuno, The Peakon Limit of the $N$-Soliton Solution of the Camassa-Holm Equation, J. Phys. Soc. Japan, **76** (2007) 034003.

[36] A. M. Kamchatnov, R. A. Kraenkel, and B. A. Umarov, Asymptotic soliton train solution of Kaup-Boussinesq equations, Wave Motion, **38** (2003) 355.

[37] G. A. El, R. H. J. Grimshaw, and N. F. Smyth, Asymptotic description of solitary wave trains in fully nonlinear shallow-water theory, Physica D, **237** (2008) 2423.

[38] V. I. Karpman, An asymptotic solution of the Korteweg-de Vries equation, Phys. Lett., **25A** (1967) 708.

[39] A. Degasperis and M. Procesi, Asymptotic integrability, edited by A. Degasperis and G. Gaeta, *Symmetry and Perturbation Theory* (Rome, World Scientific) (1999) 23.

[40] Y. Matsuno, Multisoliton solutions of the Degasperis-Procesi equation and their peakon limit, Inverse Problems, **21** (2005) 1553.

[41] Y. Matsuno, The $N$-soliton solution of the Degasperis-Procesi equation, Inverse Problems, **21** (2005) 2085.